

Effect of MgO addition on the sinterability and mechanical properties of mullite ceramics

T. A. Olcoski^{1*}, A. L. Chinelatto¹, A. S. A. Chinelatto¹

¹Ponta Grossa State University, Materials Engineering Department, Av. Carlos Cavalcanti 4748, Ponta Grossa, PR, Brazil

Abstract

Mullite is a refractory material with singular properties, although high temperatures and long sintering times are required to obtain this material with good densification. In this study, aluminum hydroxide and colloidal silica were used to produce mullite through reactive sintering and MgO was employed as a sintering additive. The compositions were prepared with different amounts of MgO and sintered at 1350, 1450, and 1550 °C, and then analyzed using X-ray diffraction, scanning electron microscopy, and measurements of apparent porosity (AP) and flexural strength. The results showed that the raw materials used allowed the mullite formation at relatively low temperatures (1350 °C), regardless of the amount of MgO added but with the increase in MgO content, a spinel phase appeared, resulting in a fraction of residual α -alumina. The MgO addition lowered the densification temperature at around 50 °C. Furthermore, the higher the sintering temperature and the MgO content, the larger and more anisotropic the mullite grains were. At sintering temperatures above 1450 °C, AP was reduced to approximately 10%. The MgO addition and increase in sintering temperature improved the flexural strength of mullite materials.

Keywords: mullite, additive, MgO, sinterability, mechanical properties.


INTRODUCTION

Mullite is a refractory ceramic of great industrial importance because of its variety of applications since it can be used in traditional applications such as dishes and refractory products as well as in advanced ones, including structural and functional applications [1-5]. Such versatility is because of its properties, namely: low thermal conductivity, low thermal expansion coefficient, high-temperature resistance, good chemical stability, low density (3.18 g/cm³), excellent creep and thermal shock resistance, high melting point, and excellent electrical resistance [1, 2, 5-10]. In the Al₂O₃-SiO₂ phase diagram, mullite is the only stable crystalline phase up to around 1800 °C under atmospheric pressure [8-11]. However, due to its high covalent bond degree, and slow diffusion of the Al³⁺ and Si⁴⁺ ions in the mullite network and grain boundaries, its production requires high temperatures, above 1600 °C, and long sintering times to achieve good densification [2, 3, 6, 7, 9]. Atisivan et al. [12] reported that mullite densification was observed at high temperatures, around 1650 °C. To reduce the material densification temperature, fine powders with submicrometer grain sizes are used, since they have a high surface area. Another possibility is to use sintering additives that promote densification through the liquid phase sintering [12]. Sintering additives help to reduce the glassy phase viscosity, making easier silicon and aluminum ions diffusion through the mullite network [3, 4, 13, 14]. The reduction in the activation energy for diffusion improves mullite

densification and reduces mullitization temperature [2, 3, 6, 7, 9, 14, 15]. This enables the production of high-density mullite at relatively low temperatures which is important for the refractory industry. Additives can also influence the morphology, microstructure, and composition of the grains [4, 14]. Many studies have been developed on the effect of additives such as MgO [2, 4, 7, 8, 15-19], TiO₂ [20], B₂O₃ [21], CeO₂ [22], Cr₂O₃ [23], La₂O₃ [7], and Y₂O₃ [2, 10, 15], on the mullitization temperature, as well as the mullite characteristics and properties after sintering [2-4, 6, 7].

Dong et al. [16] used recycled fly ash and bauxite as raw materials, with MgO addition, for mullite production. They reported that the use of MgO allowed the production of mullite at lower temperatures, around 1450 °C, in shorter sintering times and with high density and mechanical resistance. This increase in mechanical strength was attributed to the presence of large elongated and interconnected mullite crystals, associated with increased densification for samples containing MgO. Montanaro et al. [19] studied the sinterability of two industrial mullite powders, with the presence of MgO as a sintering additive. They observed the formation of a glassy phase during the process, which had a strong influence on sintering, depending on its content, composition, and distribution. They also found that, in addition to mullite, the α -alumina and spinel phases may be present, depending on the amount of MgO added. The appearance of the spinel phase occurs due to the devitrification of the liquid phase during slow cooling. MgO is one of the most studied sintering additives. The amount of MgO to be used is not well defined yet, but some studies reported that to improve the sintering behavior, amounts above 0.5% MgO in weight are needed [17, 18].

*thaysallana@gmail.com

 <https://orcid.org/0000-0002-2262-7854>

In a study by Souto et al. [3], they investigated the effect of 0.1 to 0.5 wt% MgO addition to industrial mullite. They reported that the non-doped composition sintered at 1600 °C reached 88% density, while compositions with MgO showed increased density, up to 99%. The addition of 0.5 wt% MgO also promoted a reduction in the sintering temperature from 1650 °C to approximately 1500 °C. But the formation of elongated mullite grains could only be observed when the composition was sintered at 1600 °C, and 99% density was reached [3].

Thus, the objective of this work was to study the mullitization process, sinterability, and mechanical properties of mullite produced by reactive sintering using aluminum hydroxide and colloidal silica as raw material and MgO as a sintering additive. The literature for obtaining mullite is extensive and provides information on the use of different sources for the mullite preparation, but there is no information on the use of sources such as aluminum hydroxide and colloidal silica for their production. These raw materials were chosen because colloidal silica has nanometric particles and aluminum hydroxide, upon heating, after its decomposition generates transition alumina with a high surface area, favoring the mullitization process. Furthermore, the effect of MgO addition to such materials has not been reported yet.

EXPERIMENTAL PROCEDURE

The raw materials used to produce stoichiometric mullite were aluminum hydroxide (Hidral 710, Almatís), as a source of alumina, and colloidal silica (around 30% in weight of silica, Diatom). The magnesium oxide source used was a hydromagnesite [$4\text{MgCO}_3 \cdot \text{Mg}(\text{OH})_2 \cdot 4\text{H}_2\text{O}$] with 40% in weight of MgO. The raw materials were characterized using X-ray fluorescence spectroscopy (XRF), X-ray diffraction (XRD), differential thermal analysis (DTA), and thermogravimetry (TG). The colloidal silica was characterized after drying in an oven at 110 °C for 3 h. For the characterization by XRF, hydromagnesite, and aluminum hydroxide powders were calcined at 900 °C for 1 h with a 10 °C/min heating rate to obtain MgO and Al_2O_3 , respectively. XRD was performed varying 2θ from 5° to 90° with a 2 °/min scanning speed in a diffractometer (Ultima IV, Rigaku). XRF was carried out in a spectrometer (EDX 700, Shimadzu). The DTA/TG was performed at a 10 °C/min heating rate up to 1280 °C in an air atmosphere with a thermal analyzer (STA 409 EP, Netzsch).

Different amounts of MgO were added to the mullite stoichiometric composition (71.8 wt% of Al_2O_3 and 28.2 wt% of SiO_2), as follows: 0, 0.8, 1.6, 2.4, 3.1, and 4.0 wt%. These compositions were identified as M0, M1, M2, M3, M4, and M5, respectively. The compositions were mixed in a ball mill for 6 h. Next, they were dried with hot air flow and deagglomerated in an 80 mesh nylon sieve. To evaluate the densification of the compositions with different MgO amounts, dilatometry tests were carried out. For the tests, a sample of each composition was formed using uniaxial

pressing, in a cylindrical mold. From the densification behavior, the determined sintering temperatures were used. The dilatometry was performed up to 1400 °C at a 10 °C/min heating rate, in an air atmosphere, with a dilatometer (Setsys Evolution, Setaram). To study the material sinterability, the samples were formed similarly to those used in the dilatometry. Then, the green samples were sintered at a 10 °C/min constant heating rate up to the sintering temperature (1350, 1450, and 1550 °C), with a 4 h holding time.

The sintered materials obtained from the different compositions were characterized using XRD. To verify the effect of MgO addition on the material densification, apparent porosity (AP) was measured, based on Archimedes' principle. The microstructural analysis of sintered materials was performed using field emission scanning electron microscopy (FEG/SEM, MIRA 3, Tescan). The presence and distribution of the different phases present in the sintered materials were investigated using energy dispersive spectroscopy (EDS) coupled to the FEG/SEM. To evaluate the mechanical strength of the material obtained from the different compositions and sintering temperatures, the three-point flexural test was carried out. In this analysis, the materials with low apparent porosities were chosen. Eight samples were prepared for each composition, shaped as rectangular bars; a universal mechanical testing machine (AG1 10 kN, Shimadzu) and a 1.5 mm/min displacement rate were used.

RESULTS AND DISCUSSION

Table I presents the results of X-ray fluorescence analysis of the raw materials: colloidal silica, calcined aluminum hydroxide, and calcined hydromagnesite. The results showed that the colloidal silica solid portion corresponded to 99.78 wt% of silica. The calcined aluminum hydroxide presented 99.83 wt% of Al_2O_3 and the calcined hydromagnesite presented 97.66 wt% of MgO. Fig. 1 shows the X-ray diffractograms of aluminum hydroxide, hydromagnesite, and colloidal silica. Only characteristic peaks of natural gibbsite ($\text{Al}_2\text{O}_3 \cdot 3\text{H}_2\text{O}$) were observed in the aluminum hydroxide diffractogram (JCPDS 33-0018, monoclinic aluminum hydroxide) [24]. In the hydromagnesite diffractogram, only peaks referring to the $4\text{MgCO}_3 \cdot \text{Mg}(\text{OH})_2 \cdot 4\text{H}_2\text{O}$ were identified (JCPDS 70-1177, prismatic monoclinic crystal structure). Regarding the colloidal silica, a wide and low-intensity band was observed between 15° and 30°, indicating that the silica presented an amorphous structure [25].

In Fig. 2, the curves of differential thermal analysis (DTA) and thermogravimetry (TG) of the aluminum hydroxide, hydromagnesite, and colloidal silica are presented. Fig. 2a shows approximately 43% mass loss in the TG curve because of the aluminum hydroxide decomposition, which corresponded to the endothermic peak at around 320 °C in the DTA curve [26]. In the DTA curve, a slight increase in the curve intensity can be noticed at around 1180 °C, which might indicate the transformation of θ -alumina into α -alumina, since this transformation occurs at around 1200 °C [27]. In Fig. 2b,

Table I - Chemical compositions by XRF (weight %) of the raw materials.

Oxide	SiO ₂	Al ₂ O ₃	MgO	SO ₃	Fe ₂ O ₃	CuO	CaO
Colloidal SiO ₂	99.78	-	-	0.16	0.06	-	-
Calcined aluminum hydroxide	-	99.83	-	0.09	0.06	0.01	-
Calcined hydromagnesite	0.38	-	97.66	-	0.05	-	1.91

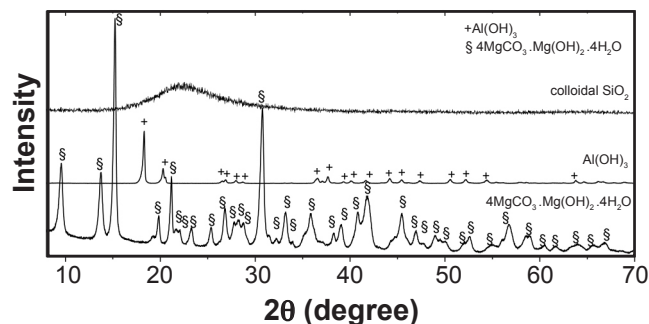


Figure 1: XRD patterns of the raw materials: aluminum hydroxide and hydromagnesite after calcination, and colloidal silica.

the transformation of hydromagnesite into magnesium oxide is observed, which is characterized by endothermic peaks occurring at around 32, 420, and 550 °C, indicated by the rectangles in the DTA curve. These peaks were attributed to the loss of hydroxyl water and carbon dioxide by magnesium hydroxide and magnesium carbonate, respectively. There was also an exothermic peak at around 500 °C, also indicated by a rectangle, which was accompanied by mass loss. This exothermic peak usually appears because of delayed recrystallization or oxidation of the products by the surrounding atmosphere [28]. The TG curve shows that the total mass loss was approximately 62.5%. Fig. 2c shows around 17.5% mass loss between 50 and 400 °C, which might be associated with the adsorbed water release in the colloidal silica particles. In the DTA curve, an endothermic peak is observed at around 150 °C because of the adsorbed water elimination, and an exothermic peak is seen at around 850 °C, associated with the amorphous silica crystallization since this transformation needs thermal energy to break the amorphous silica bonds, reorder them and form a crystalline network [29]. Nakata et al. [30] reported the appearance of an exothermic peak at around 990 °C that corresponded to the crystallization of the amorphous silica from rice hulls into cristobalite.

Fig. 3 presents the linear shrinkage rate versus temperature of the sintered compositions M0 to M5. In all compositions, there were two regions where a high shrinkage rate occurred. The first occurred between 300 and 450 °C, which was probably related to the aluminum hydroxide decomposition, due to the loss of structural water [26]. The second highest shrinkage rate occurred between 1250 and 1400 °C, which might be associated with material densification. It is important to note that for compositions M1 to M5, to which MgO was added, the maximum

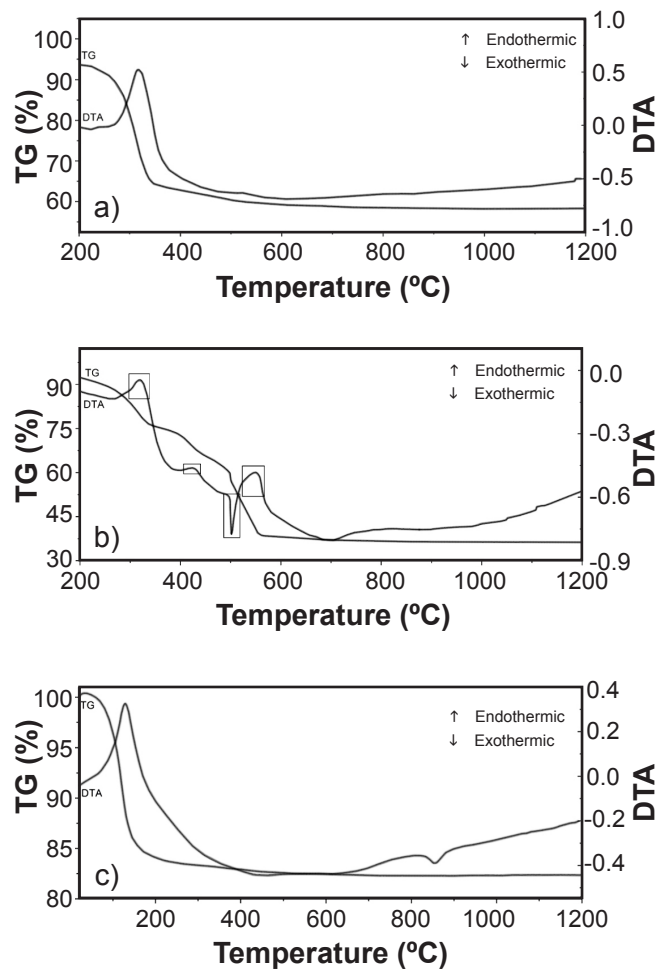


Figure 2: DTA and TG curves of: a) aluminum hydroxide; b) hydromagnesite before calcination; and c) colloidal silica, after drying at 110 °C for 3 h.

shrinkage rate occurred at lower temperatures than in the composition M0, which had no MgO in its composition. The temperature of maximum shrinkage rate for M0 was around 1380 °C, for M1 around 1340 °C, for M2 around 1330 °C, for M3 around 1335 °C, for M4 around 1300 °C, and for M5 around 1310 °C. It was observed that there was a reduction in the temperature of the maximum shrinkage rate with the increase in the amount of MgO, except for the composition M3 that presented the maximum shrinkage rate temperature almost equal to the composition M2. Montanaro et al. [13] and Dong et al. [16] also obtained similar results using other raw materials, showing that MgO addition promotes a decrease in the material densification temperature, resulting in a higher shrinkage rate at a lower temperature than the

MgO-free composition. From these results, 1350, 1450, and 1550 °C sintering temperatures, with a 4 h holding time, were chosen to continue the investigation on the mullite sinterability.

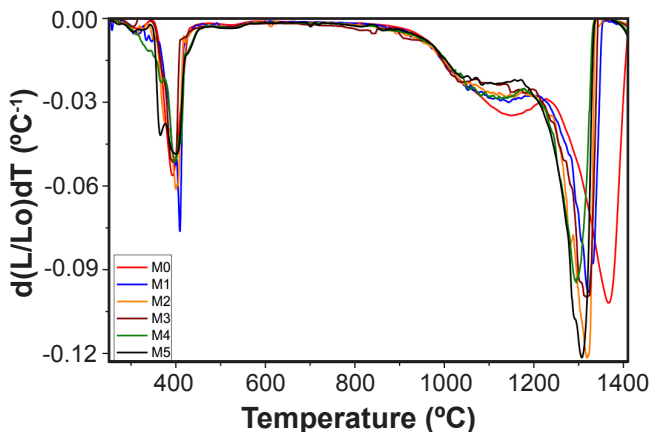


Figure 3: Linear shrinkage rate versus temperature of the compositions M0 to M5.

Fig. 4 shows the X-ray diffractograms of the materials obtained from the different compositions M0, M1, M2, and M5 sintered at 1350, 1450, and 1550 °C. The diffractograms of the compositions M3 and M4 are not shown, since they presented similar results to those found for compositions M2 and M5, respectively. For all studied compositions, regardless of the MgO content and sintering temperature, there was stoichiometric mullite formation, with composition $3\text{Al}_2\text{O}_3 \cdot 2\text{SiO}_2$ (JCPDS 15-0776, orthorhombic structure). However, only the compositions M0 sintered at 1350, 1450, and 1550 °C and M1 at 1350 °C showed only the mullite phase. The mullite formation, even at a relatively low temperature of 1350 °C, showed that the use of aluminum hydroxide and colloidal silica was efficient to promote mullitization. This fact might be associated with the small particle size and, consequently, with the high surface area of the powders used. In addition, the thermal decomposition of aluminum hydroxide also produces powders with a high surface area, which favors its reactivity. In the other compositions, for the 1450 and 1550 °C sintering temperatures, in addition to the mullite, diffraction peaks corresponding to the α -alumina phase (JCPDS 46-1212) were identified. Furthermore, for the compositions M2 to M4 sintered at 1350 and 1450 °C and M5 sintered between 1350 and 1550 °C, peaks corresponding to spinel phase (MgAl_2O_4) were also identified (JCPDS 21-1152). These results were in accordance with those found elsewhere [8, 15]. The presence of secondary phases, such as α -alumina and spinel, can be explained by a reaction between silica, alumina, and magnesium oxide. This reaction hampers the mullitization reaction at high temperatures, due to the increase in the amount of MgO [8]. Heraiz et al. [8] reported that sintering in the presence of MgO occurs through a liquid phase formed in a temperature range between 1410 and 1425 °C, according to the ternary phase diagram Al_2O_3 - SiO_2 -MgO. Viswabaskaran

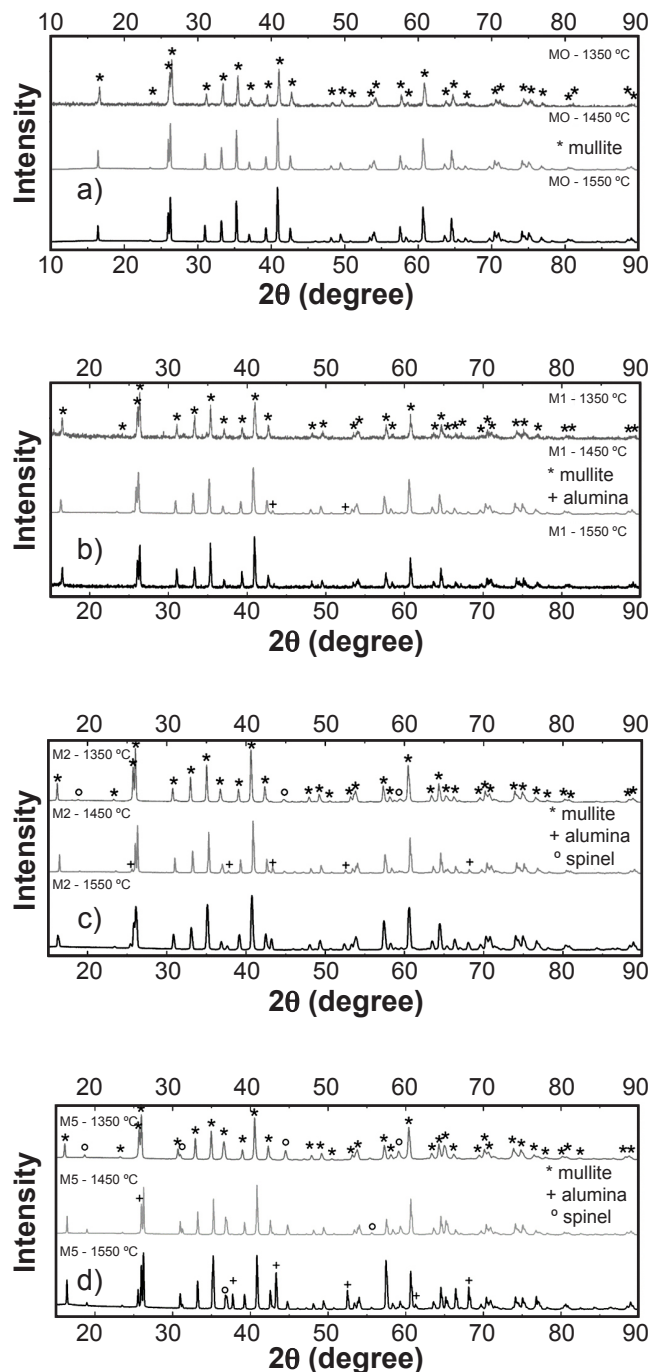


Figure 4: XRD patterns of the materials obtained from different compositions: a) M0; b) M1; c) M2, and d) M5, sintered at 1350, 1450, and 1550 °C.

et al. [15] also reported that, according to this phase diagram, the magnesium oxide might form spinel at temperatures higher than 1500 °C, but the presence of spinel grains at lower temperatures are produced as a consequence of the crystallization of the liquid phase during the material cooling. Thus, the mullite grains grow during the crystallization and end up isolating the spinel precipitates. In compositions M2 to M5 sintered at 1350 °C, peaks of mullite and spinel phases were identified, but no peaks corresponding to the residual α -alumina phase appeared in these compositions. Finally, in

the compositions M1 sintered between 1350 and 1550 °C and M2 to M4 sintered at 1550 °C, no peaks corresponding to the spinel phase were identified, which might be explained by the formation of MgO solid solution with mullite, as already reported [18].

Fig. 5 shows the apparent porosity results of the materials obtained from the different compositions M0 to M5, sintered at 1350, 1450, and 1550 °C. At the sintering temperatures of 1450 and 1550 °C, it was observed that the addition of magnesium oxide effectively reduced the porosity of compositions M1 to M5 when compared to composition M0. However, it was not possible to observe a reduction in porosity with an increase in the amount of MgO. At the sintering temperature of 1450 °C, there was a minimum point in the porosity for the composition M2, whereas, for the sintering at 1550 °C, the porosity values were practically equal for all compositions, considering the standard deviations. The reduction in porosity occurred because the MgO sintering additive promoted the generation of a low viscosity ternary liquid phase, which allowed the material densification through liquid phase sintering at high temperatures [7, 9]. Part of the porosity present in the materials obtained with the different compositions resulted from the aluminum hydroxide decomposition and in a lower proportion from hydromagnesite. When the aluminum hydroxide decomposes during heating, releasing hydroxyls from its structure, it might result in high porosity in the material microstructure [31]. It was also observed that, at the sintering temperature of 1350 °C, the addition of MgO promoted a considerable increase in porosity, indicating that the liquid phase was formed at a temperature above 1350 °C. Dong et al. [16] reported that the MgO addition is effective in mullite sinterability, mainly at temperatures above 1450 °C. Porosity in samples with MgO sintered at 1350 °C may also be associated with the presence of the alumina and spinel phases, as shown in Fig. 4, because of the different thermal expansion coefficients between these phases and mullite. The spinel and alumina thermal expansion coefficients are similar. For spinel, this value is

around $8.4 \times 10^{-6} \text{ }^\circ\text{C}^{-1}$ and for alumina is around $8.8 \times 10^{-6} \text{ }^\circ\text{C}^{-1}$ [32], however, these values are relatively higher than those for mullite, which is around $4.5 \times 10^{-6} \text{ }^\circ\text{C}^{-1}$ [13, 33].

Fig. 6 shows the SEM images of the materials obtained from different compositions M0 to M5 sintered at 1350 °C. High porosity can be observed in all microstructures, which is in accordance with the apparent porosity results presented in Fig. 5. In the composition M0, a large amount of porosity was observed between the mullite grains, forming large voids in the microstructure. The compositions M1 and M3 presented a relatively homogeneous microstructure, but also with high porosity. In the compositions M4 and M5, there was an increase in porosity distributed throughout the microstructure and the presence of acicular grains of mullite. The micrographs also showed that the greater the amount of MgO added, the more evident were the mullite grains formed. Fig. 7 presents SEM images of the materials obtained from the different compositions M0 to M5 sintered at 1550 °C. Comparing the compositions with MgO addition, M1 to M5, with the composition M0, it can be observed that the higher the MgO content added, the larger the mullite grains formed and more densified the microstructures became, which was in accordance with the apparent porosity results shown in Fig. 5. This occurred because the amount of the ternary liquid phase, which has a low viscosity above 1400 °C, increased [8, 9, 14, 15]. The addition of MgO favored the formation of the glassy phase that induced the dissolution of mullite. This dissolution occurred mainly on the high-energy surfaces of the mullite grains, which are less stable. Thus, the morphology of rounded mullite grains changed to faceted grains. In addition, during the cooling of the composition, a partial crystallization of the vitreous phase can favor a significant growth of mullite grains with faceted morphology [19]. In the M4 and M5 compositions sintered at 1550 °C, shown in Fig. 7, the microstructures show the presence of mullite grains incorporated in a glassy phase. These compositions contained higher amounts of MgO, which favored an increased liquid phase formation, reducing porosity.

Comparing the images of the compositions sintered at

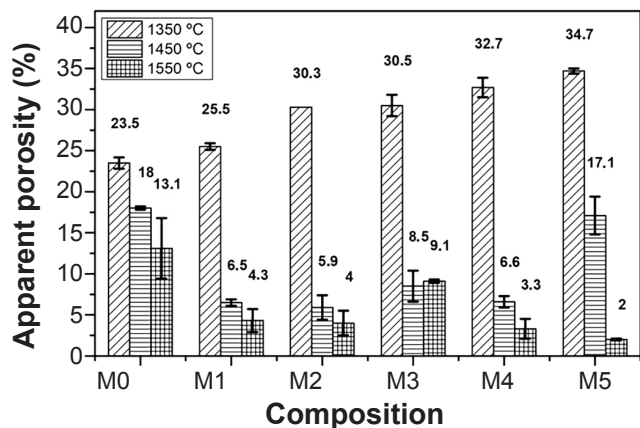


Figure 5: Apparent porosity (AP) of the materials obtained from the different compositions sintered at 1350, 1450, and 1550 °C.

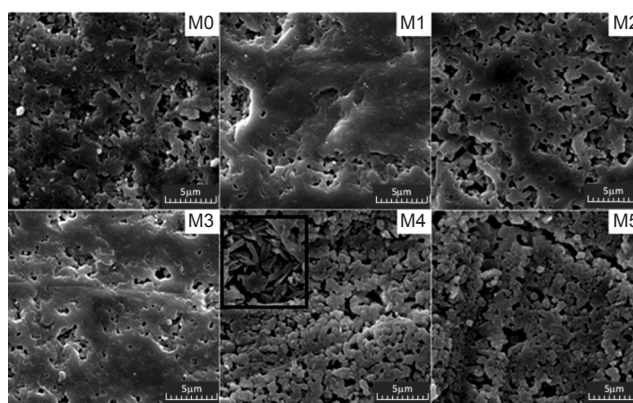


Figure 6: SEM images of materials obtained from the different compositions M0 to M5 sintered at 1350 °C.

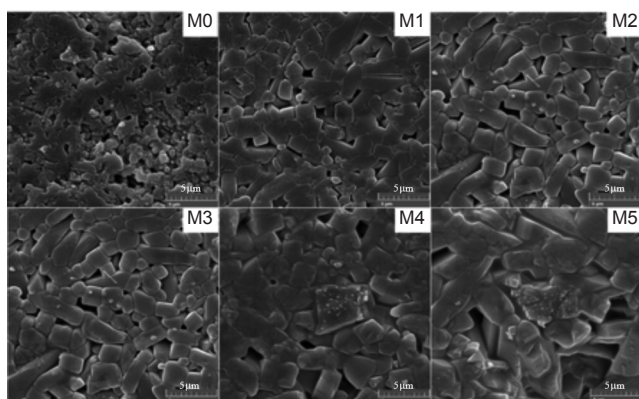


Figure 7: SEM images of the materials obtained from the different compositions M0 to M5 sintered at 1550 °C.

1350 °C (Fig. 6) and 1550 °C (Fig. 7), it can be noted that the higher the sintering temperature, the larger the mullite grains. This occurred because of higher ions diffusion coefficients with increasing temperature, which, together with the presence of MgO, accelerated the process of mullitization, in agreement with the results presented by Souto *et al.* [3]. The presence of MgO had also an effect on the mullite grain morphology. The increase in the amount of MgO produced more elongated grains, with regular boundaries, generating an interconnected structure. When MgO was added, a ternary liquid phase, rich in silica was formed at a lower temperature, and when the temperature increased, the viscosity of this liquid phase decreased, increasing the diffusion process, which consequently, accelerated the formation of anisotropic mullite grains [14]. Therefore, while the mullite grains grew, they became more elongated, which can be observed in Fig. 7.

Fig. 8 shows the mapping of chemical elements obtained using EDS to verify the phase distribution in the composition M5 sintered at 1550 °C. In the microstructure, a large concentration of Mg can be observed in small grains, with the presence of aluminum and oxygen, which might indicate the formation of a spinel phase in these grains. Some grains show a high concentration of aluminum and oxygen, which reveals the presence of α -alumina grains. The presence of the spinel and α -alumina in this composition was also seen in the XRD pattern presented in Fig. 4. The remaining elemental maps reveal homogeneous distributions of aluminum, silicon, and oxygen, confirming the presence of the mullite phase. Between some grains, high concentrations of silicon and oxygen can be observed, revealing the presence of a glassy phase interconnecting the mullite grains, according to the areas marked in Fig. 8.

Fig. 9 shows the flexural strength of the compositions M0 and M2 sintered at 1450 and 1550 °C, and M5 sintered at 1550 °C. The higher the sintering temperature, the greater the flexural strength values. It can be observed that for compositions sintered at 1450 °C, the effect of MgO addition had no significant impact on the mechanical resistance values. For compositions sintered at 1550 °C, there was a significant increase with the MgO addition. This increase

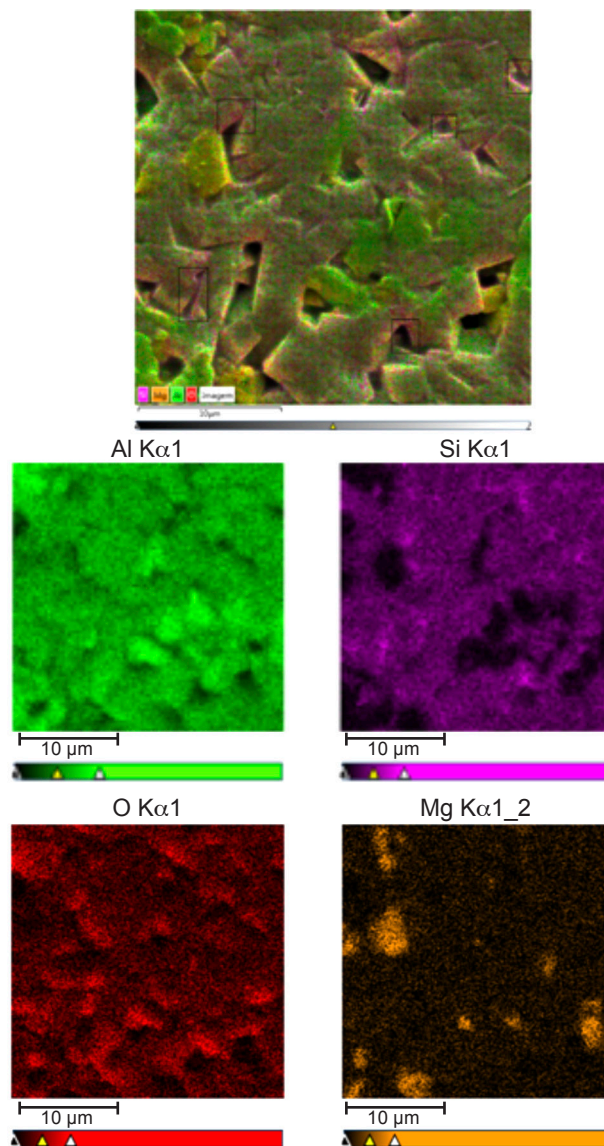


Figure 8: SEM images and mapping of the chemical elements in the composition M4 sintered at 1550 °C.

in flexural strength was associated with the formation of large elongated and interconnected mullite crystals, which appeared in the materials obtained in sintered compositions above 1450 °C. Thus, composition M5 (4 wt% MgO) sintered at 1550 °C showed the highest flexural strength, 31 MPa. In other studies, Li *et al.* [4] obtained superior values of flexural strength, around 150-169 MPa with the MgO content of 2-8 wt%, in samples with less than 0.5% porosity; Dong *et al.* [16] reached flexural strength values of 43 MPa for samples with 4 wt% MgO and 1.4% porosity. The lower mechanical strength values obtained in this study may be related to the greater porosity of the produced materials and with the presence of the glassy phase between the grains. This greater porosity was probably associated with the decomposition of raw materials used, aluminum hydroxide and hydromagnesite, which decomposed during heating, generating pores in the material's microstructure, which were not totally eliminated during the sintering of the

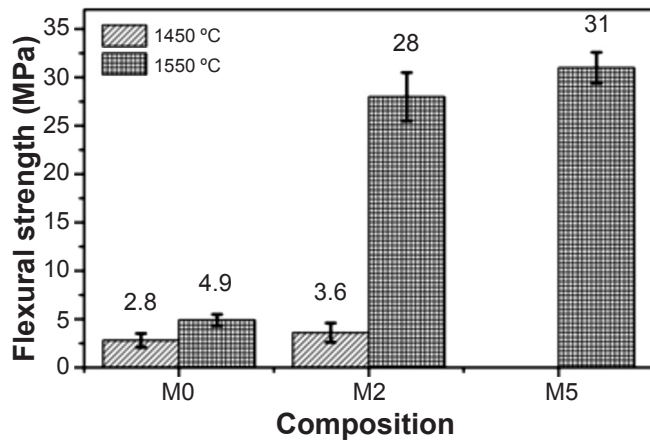


Figure 9: Flexural strength values of the compositions M0 and M2 sintered at 1450 and 1550 °C, and M5 sintered at 1550 °C.

material. Regarding the presence of the vitreous phase, it can be seen in Fig. 7 that compositions sintered at 1550 °C presented a glassy phase between the grains, which resulted in only 3% open porosity, however, their flexural strengths were relatively low when compared with other studies [4, 16]. The raw materials used in the present study made it possible to obtain mullite at relatively low temperatures, but with not so high mechanical resistance. A possibility to surmount this problem would be the calcination of aluminum hydroxide and hydromagnesite before mixing with colloidal silica, avoiding porosity caused by the decomposition of these raw materials during the sintering process.

CONCLUSIONS

Based on the obtained results, it can be concluded that the use of aluminum hydroxide and colloidal silica as raw materials allowed the mullite formation at relatively low temperatures (1350 °C), regardless of the amount of MgO added. The presence of MgO in the material densification was more effective in temperatures above 1450 °C, for promoting densification through liquid phase sintering. The higher the sintering temperature and the amount of MgO added, the larger and more anisotropic were the mullite grains produced. In compositions with content above 3 wt% MgO, the formation of a glassy phase was observed between mullite grains in the microstructures, which promoted a reduction in porosity and an increase in mechanical strength. The MgO addition and the increase in sintering temperature were beneficial for increasing the flexural strength. Therefore, the composition M5 (4 wt% MgO) sintered at 1550 °C showed the greatest flexural strength, 31 MPa, while composition M0 (0% MgO) sintered at the same temperature obtained the value of 4.9 MPa, confirming a significant increase in strength with the addition of MgO. The presence of MgO favors the mullite densification during the reactive sintering, as observed in other researches, however, the final properties, such as porosity and flexural strength depend on the raw materials used for its production.

ACKNOWLEDGMENTS

The authors thank CAPES for scholarship and C-LABMU-UEPG (Complex of Multi-Laboratory - Ponta Grossa State University) for technical support.

REFERENCES

- [1] R.M.C. Farias, R.R. Menezes, E.S. Medeiros, J.E. Oliveira, *Rev. Eletr. Mat. Proc.* **10** (2015) 1.
- [2] P.M. Souto, R.R. Menezes, R.G.H.A. Kiminami, *Cerâmica* **57**, 344 (2011) 438.
- [3] P.M. Souto, R.R. Menezes, R.H.G.A. Kiminami, *J. Mater. Proc. Tech.* **209** (2009) 548.
- [4] J. Li, L. Tong, L. Hou, J. Shen, *Adv. Mater. Res.* **295-297** (2011) 969.
- [5] V.J. Silva, E.P. Almeida, W.P. Gonçalves, R.B. Nóbrega, G.A. Neves, H.L. Lira, R.R. Menezes, L.N.L. Santana, *Ceram. Int.* **45** (2019) 4692.
- [6] G.L. de Gouveia, P.M. de Souto, R.H.G.A. Kiminami, *Cerâmica* **59**, 349 (2013) 129.
- [7] P.M. Souto, R.R. Menezes, R.G.H.A. Kiminami, *Mater. Res.* **18**, 1 (2015) 42.
- [8] M. Heraiz, A. Merrouche, N. Saheb, *Adv. Appl. Ceram.* **105**, 6 (2006) 285.
- [9] R. Sarkar, M. Mallick, *Bull. Mater. Sci.* **41**, 1 (2018) 31.
- [10] L. Yuan, B. Ma, Q. Zhu, X. Zhang, H. Zhang, J. Yu, *Ceram. Int.* **43** (2017) 5478.
- [11] L.A. Aksay, D.M. Dabbs, M. Sarikaya, *J. Am. Ceram. Soc.* **74**, 10 (1991) 2343.
- [12] R. Atisivan, S. Bose, A. Bandyopadhyay, *J. Am. Ceram. Soc.* **84**, 1 (2001) 221.
- [13] L. Montanaro, J.M. Tulliani, C. Perrot, A. Negro, *J. Am. Ceram. Soc.* **17** (1997) 1715.
- [14] Z. Hou, B. Cui, L. Liu, Q. Liu, *Ceram. Int.* **42**, 15 (2016) 17254.
- [15] V. Viswabaskaran, F.D. Gnanam, M. Balasubramanian, *J. Mater. Proc. Tech.* **142** (2003) 275.
- [16] Y. Dong, S. Hampshire, J. Zhou, Z. Ji, J. Wang, G. Meng, *J. Eur. Ceram. Soc.* **31** (2001) 687.
- [17] A. Ouali, M. Heraiz, F. Sahnoune, H. Belhouchet, M. Fatmi, N. Saheb, *Am. J. Mod. Phys.* **2**, 5 (2013) 270.
- [18] M.G.M.U. Ismail, H. Tsunatori, Z. Nakai, *J. Mater. Sci.* **25** (1990) 2619.
- [19] L. Montanaro, C. Esnouf, C. Perrot, G. Thollet, G. Fantozzi, A. Negro, *J. Am. Ceram. Soc.* **83** (2000) 189.
- [20] S.H. Hong, G.L. Messing, *J. Am. Ceram. Soc.* **81**, 5 (1998) 1269.
- [21] S.H. Hong, W. Cermignani, G.L. Messing, *J. Eur. Ceram. Soc.* **16** (1996) 133.
- [22] X. Wang, J.H. Li, L.X. Tong, W.W. Feng, *Ceram. Int.* **39** (2013) 9677.
- [23] Z. Xiao, X. Li, X. Sun, S. Yu, Y. Jiang, X. Li, H. Jiang, W. Luo, C. Wang, T. Zhang, S. Li, L.B. Kong, *J. Phys. Chem. Solids* **123** (2018) 198.
- [24] A. Malki, Z. Mekhalif, S. Detriche, G. Fonder, A. Boumaza, A. Djelloul, *J. Solid State Chem.* **215** (2014) 8.

- [25] O.S.L. Júnior, R.M. Cavalcanti, T.M. Matos, J.B. Venâncio, I.B. Barros, V.F.V. Júnior, I.C.L. Barros, *Quím. Nova* **36**, 9 (2013) 1348.
- [26] A.C.V. Coelho, H.S. Santos, P.K. Kiyohara, K.N.P. Marcos, P.S. Santos, *Mater. Res.* **10**, 2 (2007) 183.
- [27] S.G. Medeiros, R.P.S. Dutra, J.P.F. Grilo, A.E. Martinelli, C.A. Paskocimas, D.A. Macedo, *Cerâmica* **62**, 363 (2016) 266.
- [28] N. Khan, D. Dollimorey, K. Alexander, F.W. Wilburn, *Termochim. Acta* **367-368** (2001) 321.
- [29] M. Borouni, B. Niroumand, A. Maleki, *J. Solid State Chem.* **263** (2018) 208.
- [30] Y. Nakata, M. Suzuki, T. Okutani, *J. Ceram. Soc. Japan* **97**, 8 (1989) 842.
- [31] V.L. Arantes, L.L. Sousa, R. Salomão, in *60° Cong. Bras. Ceram.* (2016) 1023.
- [32] Z. Shaovei, W. Lee, *Refract. Handb.* **9** (2004) 157.
- [33] H. Scheider, J. Schreuder, B. Hildmann, *J. Eur. Ceram. Soc.* **28** (2008) 329.
(*Rec.* 17/08/2020, *Rev.* 09/11/2020, 05/12/2020, 05/01/2021, *Ac.* 07/02/2021)

